Remote Sensing in Earth Systems Sciences
https://doi.org/10.1007/s41976-019-00023-9

ORIGINAL PAPER

The Performance of Random Forest Classification Based on Phenological Metrics Derived from Sentinel-2 and Landsat 8 to Map Crop Cover in an Irrigated Semi-arid Region

Abdelaziz Htitiou[1,2] · Abdelghani Boudhar[1,3] · Youssef Lebrini[1,2] · Rachid Hadria[2] · Hayat Lionboui[2] · Loubna Elmansouri[4] · Bernard Tychon[5] · Tarik Benabdelouahab[2]

Received: 1 May 2019 / Revised: 26 August 2019 / Accepted: 20 September 2019

Abstract

The use of remote sensing data provides valuable information to ensure sustainable land cover management. In this paper, the potential of phenological metrics data, derived from Sentinel-2A (S2) and Landsat 8 (L8) NDVI time series, was evaluated using Random Forest (RF) classification to identify and map various crop classes over two irrigated perimeters in Morocco. The smoothed NDVI time series obtained by the TIMESAT software was used to extract profiles and phenological metrics, which constitute potential explanatory variables for cropland classification. The method of classification applied involves the use of a supervised Random Forest (RF) classifier. The results demonstrated the capability of moderate-to-high spatial resolution (10–30 m) satellite imagery to capture the phenological stages of different cropping systems over the study area. Furthermore, the classification based on S2 data presents a higher overall accuracy of 93% and a kappa coefficient of 0.91 than those produced by L8 data, which are 90% and 0.88, respectively. In other words, phenological metrics obtained from S2 time series data showed high potential for agricultural crop-types classification in semi-arid regions and thus can constitute a valuable tool for decision makers to use in managing and monitoring a complex landscape such as an irrigated perimeter.

Keywords Phenological metrics · Random forest · Crop mapping · Classification · Landsat 8 · Sentinel-2

Abbreviations

NIR	Near infrared
SWIR	Shorter wave infrared
VRE	Vegetation red edge

✉ Abdelaziz Htitiou
abdelazizhtitiou@gmail.com

1 Water Resources Management and Valorisation and Remote Sensing Team, Faculty of Sciences and Technology, Sultan Moulay Slimane University, Beni Mellal, Morocco

2 Natural Resources and Environment Department, National Institute of Agronomic Research, Rabat, Morocco

3 Center for Remote Sensing Applications (CRSA), Mohammed VI Polytechnic University, Ben Guerir, Morocco

4 College of Geomatic Sciences and Surveying Engineering, Hassan II Institute of Agronomy and Veterinary Medicine, Rabat, Morocco

5 SPHERES Research Unit, Faculty of Sciences, University of Liege, Arlon Campus, Arlon, Belgium

1 Introduction

Irrigated areas in semi-arid regions play a strategic role in food security, providing more than half foodstuffs produced in the world [4, 49]. In Morocco, irrigated agriculture significantly contributes to the process of economic and social development, in spite of its area of only 15% of the cultivated land (about 1.5 million ha). It accounts for 45% of the agricultural Gross Domestic Product and 75% of agricultural exports, depending on the season [7, 47]. Within this framework, a strong mobilization of decision-makers has been created to establish an institutional reform, and an agricultural policy for monitoring and managing land use and land-cover efficiently in the irrigated areas.

In this context, remote sensing can be an effective tool for identifying and monitoring of crop types in agricultural regions. Several studies have commonly utilized multi-spectral data from a single date as an input to traditional maps of different cropping systems [34, 51, 56]. This approach captures the specific spectral response of crop types based on only one date in time. This can induce confusion

Published online: 29 October 2019

between crop types caused by their spectral similarity at specific phenological stages ([2, 48]).

More recently, efforts have focused on the use of multi-temporal data, which has proven to be appropriate for monitoring and characterizing spatial and temporal patterns of crop cover changes. Taking advantage of the repeat acquisitions, time series data improve the accuracy compared to single-date mapping approaches [26, 77, 82].

The time series of multispectral data from sensors such as Landsat Thematic Mapper (TM and ETM+) and SPOT were used by many researchers at the local scale for detailed crop mapping [15, 40, 60, 79]. However, the computation time and memory management of the acquired full multispectral data during the whole cropping season are not practical due to the large data volume.

To overcome this problem, many studies have been using several vegetation indices that are derived from satellite data to identify agricultural land cover classes [1, 31, 58, 64, 71, 81, 82, 84]. Furthermore, various studies proved that the Normalized Difference Vegetation Index (NDVI), developed in the early 1970s [68, 75], correlates with plant productivity [75]. This makes the NDVI a good indicator of measuring changes in aboveground biomass and phenology [3].

The time series of vegetation indices derived from remote sensing image data has allowed researchers to quantify and characterize seasonal events of plant phenological profiles according to its seasonal patterns [62]. TIMESAT software was used to estimate the main phenological events for each pixel using the NDVI time series [38, 39]. Thirteen phenological parameters, which represent the main phenological events, were derived from phenological profiles. Several studies that used these parameters to identify and discriminate crop types at the pixel level have been based on coarse resolution satellite data, including AVHRR data [32], MODIS data [38, 44], and PROBAV datasets [20, 27]. However, the high temporal and spatial resolution of USGS Landsat 8 OLI and Copernicus Sentinel 2 sensors has opened up important opportunities for extracting these phenological metrics at finer spatial resolution.

In order to produce a final crop map for a specific season, it is necessary to use an image classification strategy as one of the most important application in remote sensing which aims to label each pixel in the image to a certain crop class. The crucial prerequisite for a successful cropland mapping is the right choice of a suitable classification method, image analysis approach, and pixel's attributes [23, 50]. A multitude of classification algorithms have been developed to map crop type classification with remote sensing time series data. These methods can be broadly categorized into three main types: unsupervised classifiers, such as ISODATA [11, 78]; parametric supervised classifiers such as maximum likelihood [18]; and non-parametric supervised machine learning classifiers which include decision trees [24, 57], artificial neural networks [41], and the support vector machines [84].

Random Forest (RF) is one of the most recent machine learning algorithms [12], which has received increasing attention in the literature over recent years due to its numerous advantages ([6]a). Some of these advantages include the low sensitivity to feature [67], the fast processing speed [54], and its robustness and stability. This approach is close to those of the Extra-Trees algorithm [22, 59]. In addition, RF showed promising results on crop mapping [5, 31, 34, 35] by exploiting its strengthened resilience and adaptation capacity for the classification of heterogeneous crop types over large areas by using remotely sensed data [26].

In irrigated arid and semi-arid regions in Morocco, crop cover changes monitoring provide important data for ensuring a sustainable agricultural land cover management. Thereby, the main objectives of this study are (i) to assess and compare the performance of phenological metrics derived from L8 and S2 data to map crop types in the Tadla and Triffa irrigated perimeters in Morocco and (ii) to evaluate the accuracy of RF algorithm as a classifier based on phenological metrics.

2 Materials

2.1 Study Areas and Ground Data

This research focuses on the irrigated perimeters of Tadla and Triffa. These particular perimeters were chosen due to several considerations, namely the strategic role in the national food security and the similar climatological and environmental conditions.

The first area of study is Tadla's irrigated perimeter, which has an area of 97,000 ha, and is located between the latitudes 31°00′ and 33°00′ North and the longitudes 5°00′ and 9°00′ West in the Beni Mellal-Khenifra Region in Morocco's center (Fig. 1). The Oum Er'Rbia River crosses this plain throughout its length dividing it into two large irrigated independent perimeters: Beni Moussa (69,500 ha) on the left bank and Beni Amir (27,500 ha) on the right bank. The area has a semi-arid climate with an average annual rainfall of 300 mm for the period of 1970 to 2010 and a mean annual temperature of around 19 °C [55].

The second area of study is Triffa's irrigated perimeter, which has an average altitude of 200 m above the sea level and an area of 36,600 ha. Triffa's irrigated perimeter is one of the most fertile and productive areas in eastern Morocco. This study area is located within the province of Berkane and lies between latitudes 34°20′–36°00′ N and 2°10′–2°40′ W. It is limited by the Beni-Snassen mountains to the south, the Ouled Mansour hills to the north, the Kiss River to the east, and the Moulouya River to the west. The climate is semi-arid with total annual rainfall below 327 mm/year and concentrated between January and April. The mean annual temperature is 17 °C, but seasonal variability is high with a monthly

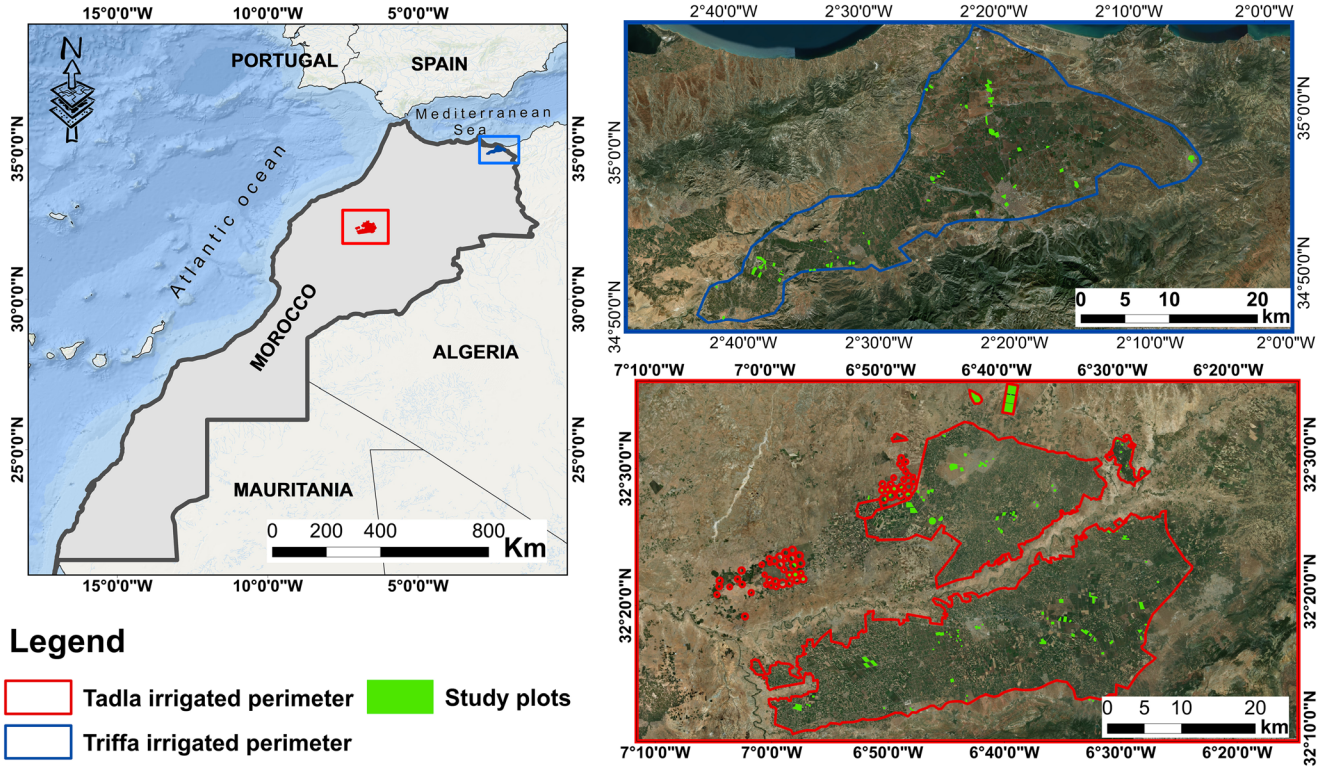

Fig. 1 Map showing location of study areas, including the Triffa (top right) and Tadla (bottom right) irrigated perimeters in Morocco. The green patterns on the images are distributions of ground reference data

temperature ranging from 11 to 25 °C. The average annual actual evapotranspiration is approximately 1200 mm/year.

In this study, ground data include different types of land cover elements and crops. These data were collected through extensive field surveys carried out in the frame of the Anillo Project Competitive Mechanism for Research and Development and Extension (MCRDV) in the two studied perimeters (Table 1). This campaign took place during the 2016–2017 agricultural season, at the same time as the acquisition of the satellite images that are used to map major crops and land cover types such as citrus, sugar beet, cereals (wheat and barley), fallow, bare soil, urban area, pomegranate, olive tree, rosaceae trees (apple, apricots, pear and peach), alfalfa, vineyard, and vegetables (mostly potatoes). In total, 240 polygons are collected covering the area of 446 and 1651 ha (ha) in Triffa and Tadla irrigated perimeter, respectively (Table 1).

The ground data used in the mapping was randomly split into two independent parts, and 80% of the samples were assigned to the initialization of the classification model, while 20% of the remaining samples were used for validation and assessment of the model performance.

2.2 Satellite Images

In this study, we used satellite data, acquired by two different sensors, Sentinel-2A MSI (S2) and Landsat 8 OLI (L8), to determine crop cover types. L8 satellite was launched in February 2013. The Operational Land Imager (OLI) sensor on board provides eight spectral bands with a spatial resolution of 30 m and one panchromatic band with a resolution of 15 m and a repeat overpass every 16 days as illustrated in Table 2 [36].

Table 1 Total area of crops collected during the ground survey

Study areas		
Classes	Training area in Tadla (Ha)	Training area in Triffa (Ha)
Citrus	254	87
Sugar beet	240	12
Cereals	145	55
Fallow	131	42
Bare soil	–	15
Urban	49	44
Pomegranate	16	88
Olive	728	21
Rosaceae	–	28
Alfalfa	88	10
Vineyard	–	34
Vegetables	–	10
Total	1651	446

The second satellite data used in this study is the European Sentinel-2A, launched in June 2015, S2 carries the Multispectral Instrument (MSI) which has spectral response functions quite different compared to its predecessor with 13 spectral bands and three different spatial resolution as well as 10 days between revisiting time (Table 2) [19].

To analyze the dynamics of vegetation in the study areas, a time series of 26 suitable images with less than 20% cloud cover from each sensor (L8 and S2) were acquired respectively via the United States Geological Survey (USGS) on-demand interface (ESPA) (https://espa.cr.usgs.gov), and the Theia land data center from July 2016 to August 2017 for both study areas. The L8 acquired images were already atmospherically corrected (level 2A) by the Landsat Surface Reflectance Code (LaSRC) algorithm [76], from which NDVI index can be derived and downloaded as a single band product. The Theia website provides S2 data in the form of 13 separate spectral bands corrected from atmospheric and slope effects (processing level 2A) thanks to the MACCS-ATCOR Joint Algorithm (MAJA) [28–30]. Then NDVI layers were generated for each image using red and near-infrared spectral bands according to the following equation [75]:

$$NDVI = \frac{NIR - RED}{NIR + RED} \quad (1)$$

where NIR and RED are the reflectance measured in the near-infrared and red bands for each pixel, respectively.

3 Methodology

A schematic workflow of the methodology applied in this study is given in Fig. 2. First, we reconstructed the smoothed NDVI time series from the L8 and S2 product using Timesat software to extract phenological metrics from the smoothed curve. We then exploited the Random Forest (RF) algorithm to calculate an importance score for all the phenological metrics for each satellite time series data. Therefore, we select the most important features for the classification of the seasonal metrics derived from the S2 and L8 time series based on the mean decrease in accuracy (MDA). Furthermore, the RF algorithm was used to classify crop types based on the most important phenological parameters. And, finally, we assess the classification accuracy and performance for each crop and each sensor.

3.1 Reconstructing NDVI Time-Series

To reduce noise introduced by unfavorable atmospheric conditions and undetected clouds, the original NDVI time series was smoothed using the Savitzky–Golay (S–G) filter [14, 70], implemented under the TIMESAT program [38] along with two other methods to smooth the time series NDVI (asymmetric Gaussian functions (A-G) and double logistic functions (D-L)). The S–G method maintains and preserves the NDVI profile by using a moving window, which eliminates the outliers and corrects the errors present in the time series of NDVI [14]. The general equation (Eq. (2)) of the S–G filter is:

Table 2 Characteristics of Sentinel-2A(MSI) and Landsat 8 (OLI) sensors

	Sentinel-2A(MSI)		Landsat 8 (OLI)	
Bands	Spectral range (μm)	Spatial resolution (m)	Spectral range (μm)	Spatial resolution (m)
Coastal/aerosol	0.43–0.45	60	0.43–0.45	30
Blue	0.46–0.52	10	0.45–0.51	30
Green	0.54–0.58	10	0.53–0.59	30
Red	0.65–0.68	10	0.64–0.67	30
VRE-1	0.70–0.71	20	–	–
VRE-2	0.73–0.74	20	–	–
VRE-3	0.77–0.79	20	–	–
NIR	0.78–0.90	10	–	–
NIR narrow	0.85–0.87	20	0.85–0.88	30
Water vapor	0.93–0.95	60	–	–
Cirrus	1.37–1.39	60	1.36–1.38	30
SWIR-1	1.57–1.66	20	1.57–1.65	30
SWIR-2	2.10–2.28	20	2.11–2.29	30
Pan	–	–	0.50–0.67	15

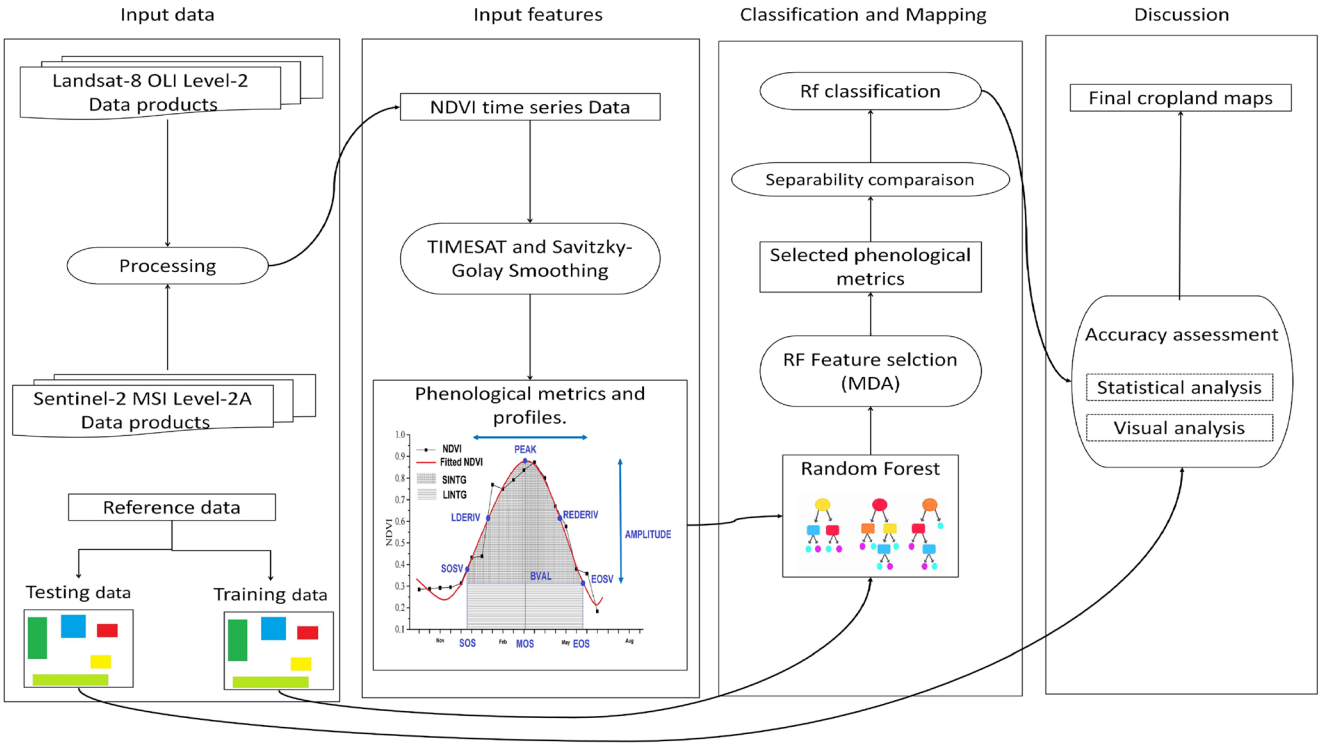

Fig. 2 Workflow of the methodology applied

$$g_{\mathrm{i}} = \frac{\sum_{n=-nL}^{nR} C_{\mathrm{n}} f_{\mathrm{i+n}}}{n} \tag{2}$$

where f_{i} represents the original NDVI value in the time series, g_{i} is the filtered NDVI value, and n is the width of the filter window, while nL and nR correspond respectively to the left and right edge of the signal component.

The idea of this filter is to preserve high moments within the data (Press 1992). Therefore, in Eq. (3), the c_{n} is not a constant, but a quadratic polynomial function depends on the user's preference and is used to fit each data value f_{i} in the moving window:

$$c_{\mathrm{n}}(t) = c_1 + c_2\, t + c_3 t^2 \tag{3}$$

where t corresponds to the time in days of the year in NDVI time series.

In this paper, the window size is set to 4. This corresponds to an optimal and balance value between the degree of smoothing and the maintenance of the trend of the original time series [14, 21]. The result of the S–G smoothing method is shown in Fig. 3.

3.2 Extracting Phenological Metrics

After smoothing the NDVI time series with the S–G filter, the phenological metrics were obtained for each pixel using the TIMESAT program. Thirteen phenological metrics can be extracted from the smoothed NDVI time series by the commonly used dynamic threshold methods, which deduce that when the NDVI values exceed a given threshold, a specific phenology phenomenon has been established [38, 62]. The start (SOS) and end (SOS) of the season are the time when the NDVI increased or decreased to a dynamic threshold (10% of the seasonal amplitude), and the length of the season (LOS) as the difference between EOS and SOS [21]. The large integral (LINTG) is an estimate of total vegetation production from the zero level, whereas the small integral (SINTG) is a measure of the vegetation production within a growing season or net primary production, calculated above the base value (BVAL) [21]. The other phenological metrics that were detected, and their definitions, are listed in Table 3 and depicted in Fig. 3.

3.3 Random Forest Classification and Feature Selection

For each irrigated perimeter, the classification was performed by the Random Forest (RF) algorithm, a non-parametric supervised learning method that is part of the machine learning classifiers. This classification method is constituted by a set of decision tree classifiers, in which each individual decision tree is randomly constructed using a bootstrap sample from two-thirds of the original training data, while the remaining one third, known as the out-of-bag (OOB) samples, are used to obtain an internal error estimate [6, 12]. Subsequently, each

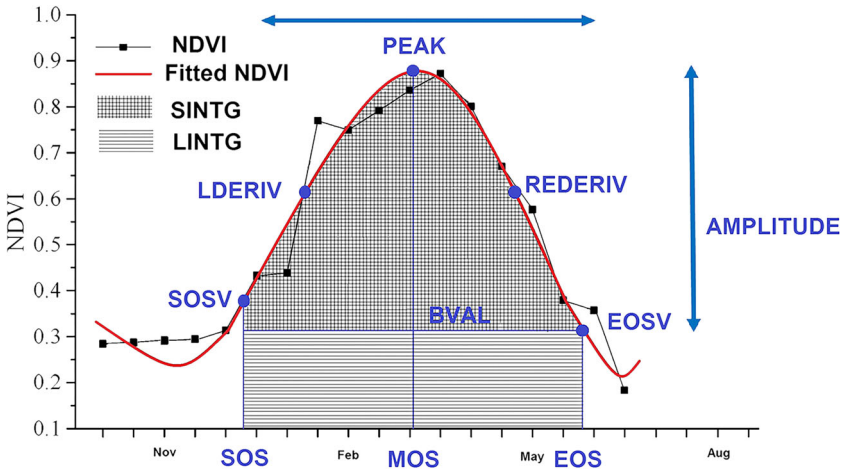

Fig. 3 Seasonality metrics extracted by TIMESAT

tree classifier casts a single vote for a specific class, and the final result was the class which had the highest number of votes by tree classifiers [12, 46, 66].

The main metrics of the RF models are the maximum number of decision trees to generate in the forest (ntree) and the number of variables used to split each node (mtry). In this study, a sufficiently high number of 500 decision trees were used in the RF modeling and a default value of mtry, which corresponds to the square root of the number of variables as recommended by Belgiu and Drăguț [6] and Bernard [10].

The RF model proposed makes it possible to transmit information on the variables used in the classification. This information gives a general idea of the ideal variables necessary to explain the result of the classification. Therefore, it is necessary to optimize the number of features for the RF model. Ranked from the more to the less important, the optimization phase was based on an analysis of the importance of the variables used on the resulting overall classification accuracy.

In this study, the procedure of selecting and ranking key features was determined using the Mean Decrease Accuracy (MDA) according to the methodology described by Immitzer et al. [34]. The MDA for a given variable consists of evaluating the internal error OOB of the classification before and after a random permutation of the values of the variable. If a large decrease in the OOB error is observed, then the importance of the feature in classification is higher [12, 33]. The majority of the studies reported by Belgiu and Drăguț [6] used the MDA to determine the variable importance, and to further reduce the size of the dataset by removing uninformative variables with the lowest ability to discriminate between the crop classes over the whole study areas.

Table 3 Seasonality metrics in TIMESAT

Phenological metrics	Abbreviation	Description
Start of season	SOS	Time for which the left edge has increased to 10% of the seasonal amplitude measured from the left minimum level
End of season	EOS	Time for which the right edge has decreased to 10% of the seasonal amplitude measured from the right minimum level
Middle of season	MOS	Mean value of the times for which the left part of the NDVI curve has increased to the 90% level and the right part has decreased to the 90% level
Length of season	LOS	Time from the start to the end of the season
Base value	BVAL	The average of the left and right minimum values
Maximum value	PEAK	Maximum NDVI value for the fitted function during the season
Amplitude	AMPL	Difference between the peak value and the base level
Large integral	LINTG	The area under the smoothed curve between SOS and EOS
Small integral	SINTG	The area below the base level from the SOS to the EOS
Left derivative	LDERIV	Rate of increase at the SOS between the left 10% and 90% of the amplitude
Right derivative	RDERIV	Rate of decrease at the EOS between the right 10% and 90% of the amplitude
Start of season value	SOSV	NDVI value at the defined start of season
End of season value	EOSV	NDVI value at the defined end of season

3.4 Crop Separability

Classification performance depends on four key factors: class separability, training sample size, dimensionality, and classifier type. In order to characterize the behavior of the phenological parameters, the studied crops boxplots and 2D feature space plot methods were visually analyzed to evaluate their separability and the ability of these parameters to discriminate the crops. These graphical techniques illustrate how training data are distributed across phenological metrics related to L8 and S2. The isolated point clouds, resulted from the scatter plot, indicate the capacity of phenological parameters to detect the behavior of the crops phenological signature.

3.5 Accuracy Assessment

The accuracy of the classification results obtained was evaluated using the testing parcels (20% of total ground data) collected during the field visits (Table 1). The accuracy statistics for these two irrigated areas were calculated on the confusion matrix that included overall accuracy (OA), Kappa coefficient, producer's accuracy (PA), user's accuracy (UA), and F1-score [16, 17].

4 Results and Discussion

4.1 Optimal Feature Selection and Crop Separability

The temporal pattern of the smoothed NDVI profiles derived from S2 and L8 datasets throughout the 2016–2017 cropping season is shown in Fig. 4. These profiles describe the phenology of randomly selected pixels for major crop types over the two study areas.

Figure 4 illustrates slight differences among NDVI derived from the two sensors for the same class of crops. The most logical explanation for this distinctness could be given to directional effects, the atmosphere characteristics, and the different illumination and viewing angle depending on the sensor's orbital parameters, which is consistent with the findings in recent studies [63, 69].

The analysis of NDVI profiles shows a clear difference between the crop types (Fig. 4). It allows us to characterize and discriminate annual crops (cereals, sugar beet, vegetables, and fallow) and perennial crops (citrus, olive, and pomegranate). Annual crops exhibit a distinct cyclic annual (sinusoidal) behavior and high amplitude [65] related to crop types, climatic and edaphic conditions [37]. Perennial crops are characterized by more stable phenological behavior throughout the crop year and low amplitude for most classes [9].

Previous studies have generally reported that the distinction between different crops can be made visually based solely on the form and size of their NDVI temporal profiles [13, 31, 45]. These profile shapes, derived from the NDVI time series, can be exploited to derive a set of indicators (metrics) that describe the form and size of these profiles (see Sect. 3.2) and reflect the appearance of certain events in the plant life cycle, which correspond to all the phenological metrics described above.

The various phenological metrics that are available in TIMESAT were evaluated to select the most useful in discrimination of different types of crops using the MDA technique [25]. Figure 5 displays the most important features for the classification of the seasonal metrics that are derived from the S2 and L8 time series based on MDA index. An analysis of the variable ranking shows that, for the MDA index, the EOS is the most frequently used variable in the phenological S2 data followed by the SOS and the SOSV. For the phenological L8 data, the SOSV and BVAL were identified as the two most important metrics used in the classification, closely followed by other metrics (i.e., LINTG, EOSV, and SINTG; Fig. 5). The least four important variables (LOS, LDERIV, RDERIV, and PEAK) were successively removed to obtain a final dataset of nine informative variables, which was used for the model classification. In general, similar results were reported by Steenkamp et al. [73] in South Africa using AVHRR data. Their results indicated that the RDERIV, LDERIV, and the PEAK were the less important metrics for distinguishing between biomes, which is consistent with our findings for both sensors, as shown in Fig. 5.

Figure 6 presents boxplots for the visualization and the statistical analyses of the nine optimal phenological metrics derived from each sensor as shown below. The boxplots show that phenological metrics have revealed different growth patterns of each studied crops, which help to ensure good discrimination between cropland classes of the study area by a random forest classification.

As indicated in Figs. 6 and 7, the distribution of phenological metrics derived from the smoothed S2 and L8 NDVI time series has the same behavior globally for each crop type and differences are much smaller between the two sensors as seen previously with the temporal profiles (Fig. 4). In general, different crop types are clearly distinguished in most cases. The classes of vineyard, rosaceae, alfalfa, and vegetables show higher values in the SOS, EOS, and MOS metrics compared to other classes (Fig. 6); this pattern can be explained by the different timing of phenological events caused by their nature as a deciduous crop (vineyard and the rosaceae). Also, their photosynthetic activity obviously starts in late March, as NDVI sees rapid increases and reaches their peak around June. Senescence phases of these classes occur in late October with a rapid decrease in NDVI value due to losing their leaves in this date. For the alfalfa, the difference in phenological timing (SOS, EOS, and MOS) could best be explained by agricultural practices carried out on the parcels (grazing, cutting…) during the year. We also found that

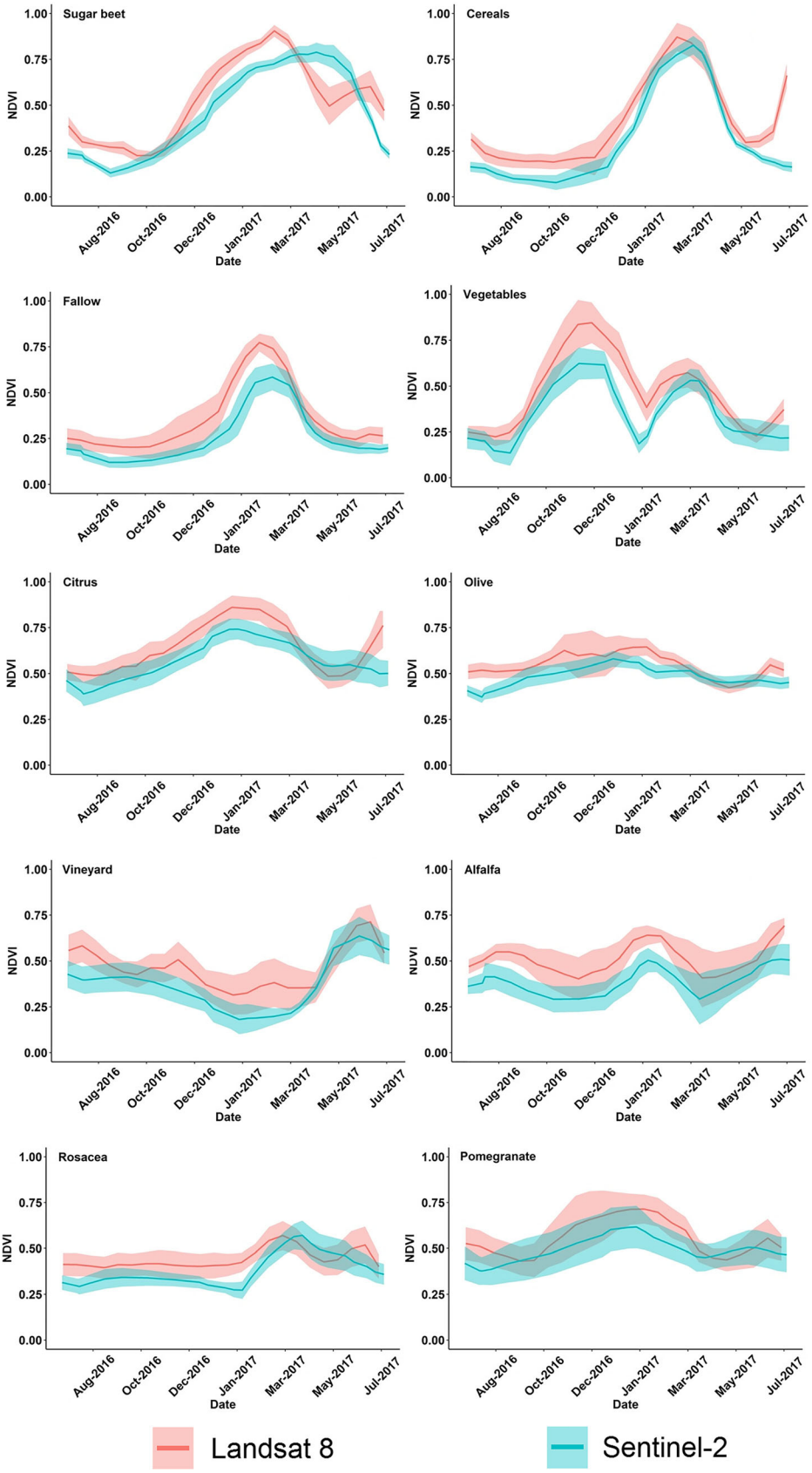

Fig. 4 Smoothed L8 asnd S2 NDVI profiles (July 2016 to August 2017) shown the NDVI evolution of major crop classes used for classification in this study

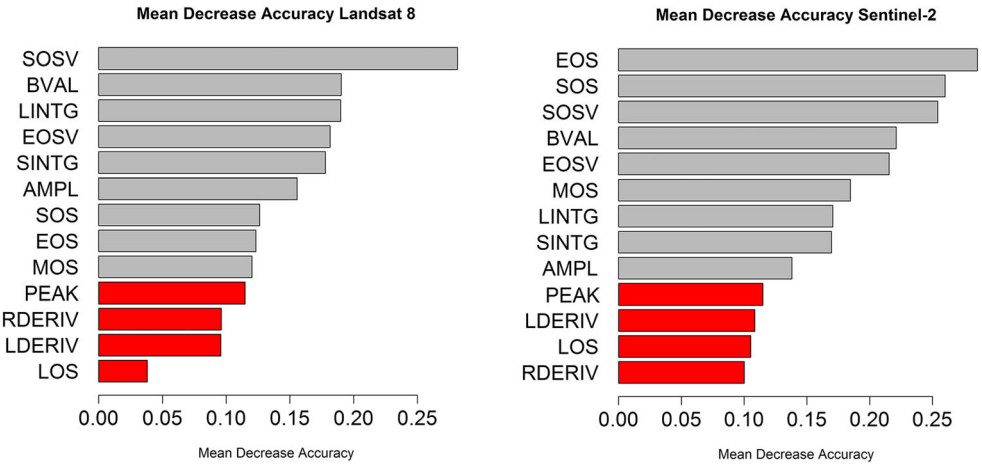

Fig. 5 Variable importance contribution of different Sentinel-2 and Landsat 8 phenological metrics in terms of OOB mean decrease in accuracy

BVAL, the average of the two seasonal minima [39], showed the largest distinction between the groups of citrus, olive, and alfalfa with a high value of BVAL and a stable spatio-temporal vegetation evolution compared to other crops, like cereals and fallow that are more distinguished by a high peak due to their increased canopy biomass which is preceded and followed by a rapid decline in photosynthetic activity, showing as a decrease in the NDVI profile back to the lowest BVAL (Fig. 6).

The phenological metrics of AMPL and SINTG show almost the same behavior against the major crops studied (Figs. 6 and 7). These metrics are considered as productivity-related parameters that describe the seasonally active vegetation or seasonal change in net primary production [39], which can be large for annual crops and herbaceous vegetation and small for the evergreen cover types. This specific behavior of AMPL and SINTG is proven by the higher value of annual crops (cereals, sugar beet, fallow, and vegetables) that make this discrimination particularly pronounced.

The LINTG is also a productivity-related parameter with a phenological interpretation as the total of vegetation production [83]. The larger integral value observed for the perennial crops (citrus, olive, and pomegranate) indicates more biomass production, but the annual net productivity might not be that much for these woody plants, which is clearly detected by the low value in SINTG and AMPL. This is consistent with Qin [61], who observed that sparse grasslands have less LINTG

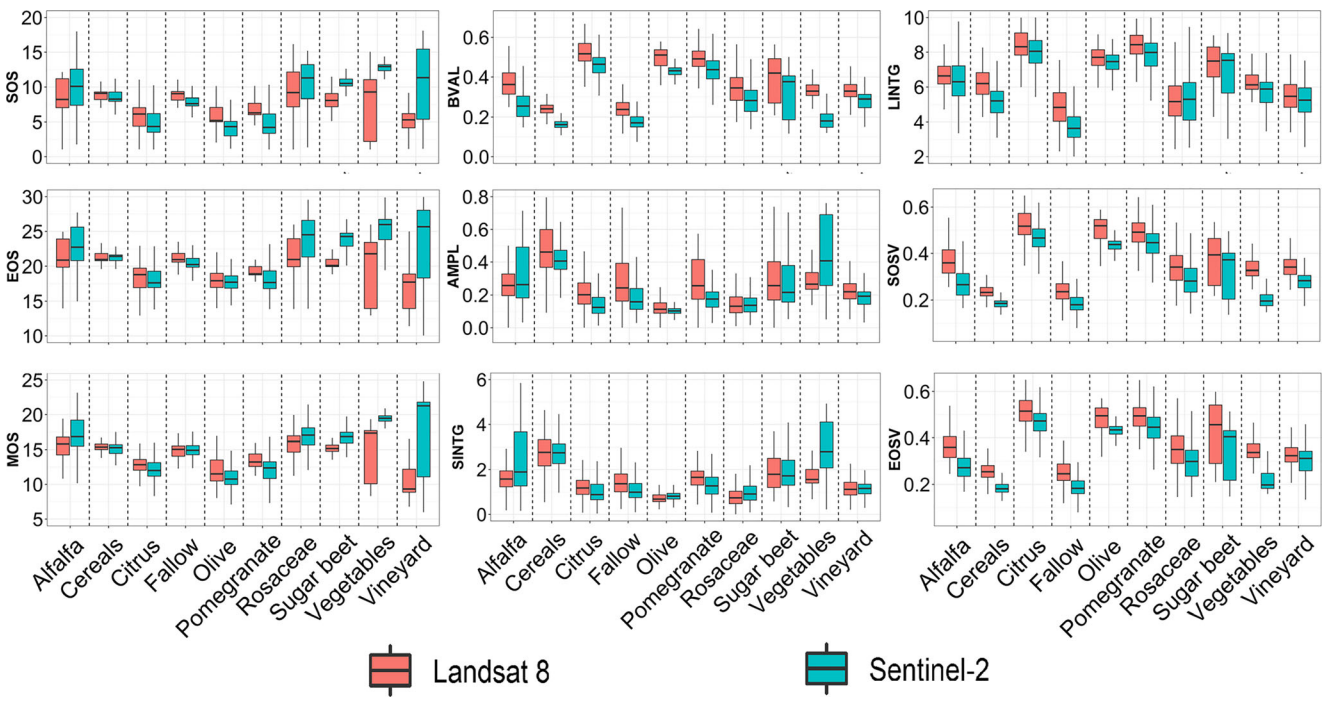

Fig. 6 Boxplots showing the distribution of each of the phenological metrics obtained with TIMESAT, for each crop and sensor types (L8, S-2) over the 2016/2017 cropping season

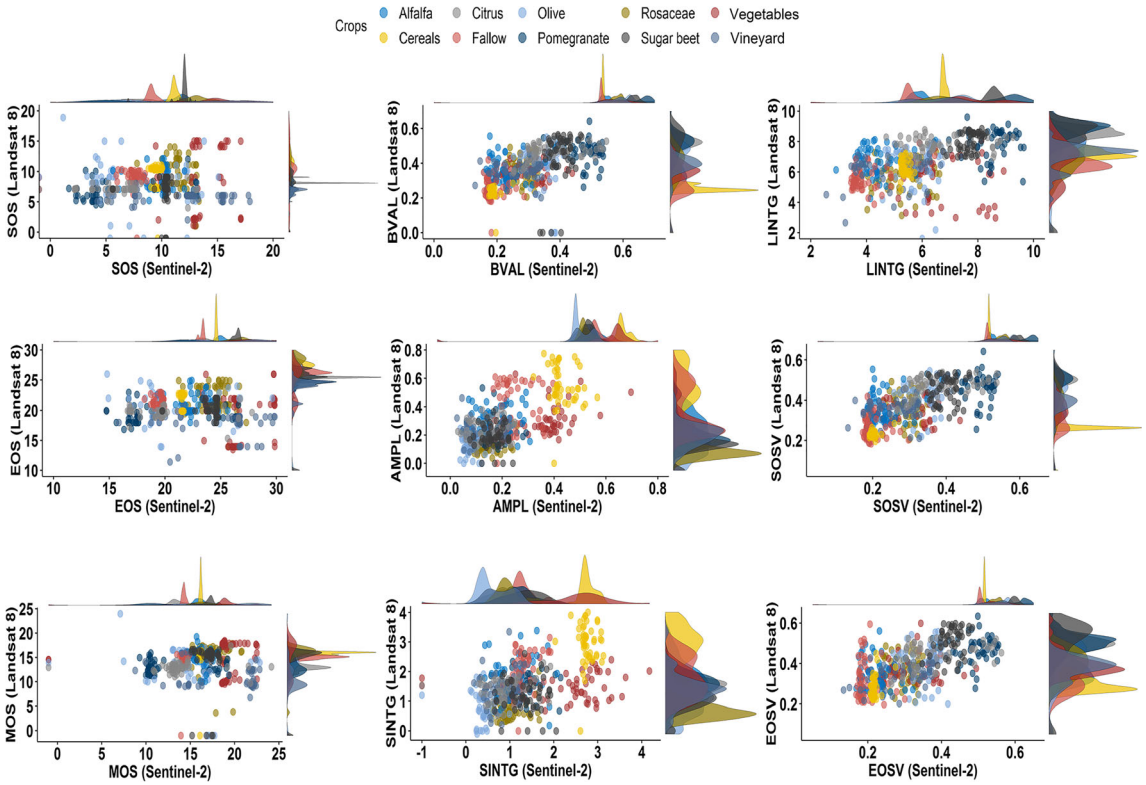

Fig. 7 Feature space plots showing the distribution of the phenological metrics of S2 v sL8

than the wooded grassland and the woodland has a higher LINTG with a low SINTG.

The SOSV and EOSV metrics have almost the same pattern inverse to the crop classes. It is very clear that there is not a lot of overlap between the different crops, making it simple to differentiate between them (Fig. 7). The groups of citrus, olive, and pomegranate show high values compared to annual crops (Figs. 6 and 7), which have a low value of NDVI correlating to the date of emergence and harvest, as well as to the dry season in which herbaceous plants either decline or dormant [53].

Table 4 Accuracy descriptive statistics

Classes	Sentinel-2			Landsat 8 (OLI)		
	PA (%)	UA (%)	F1-score (%)	PA (%)	UA (%)	F1-score (%)
Citrus	85	88	87	76	85	80
Sugar beet	96	97	97	97	96	96
Cereals	98	98	98	94	94	94
Pomegranate	57	89	69	37	72	49
Alfalfa	76	97	85	70	88	78
Olive	97	92	94	97	89	93
Bare soil	55	87	67	61	100	75
Fallow	94	83	95	92	91	91
Vegetables	93	96	95	68	79	73
Rosaceae	87	83	85	65	73	68
Urban	94	83	88	99	87	92
Vineyard	96	95	96	97	92	90
Kappa	0.91			0.88		
OA (%)	93			90		

4.2 Crop Classification Results

The results of the extraction and selection of phenological metrics are elementary data for the development of the classification models. With two different data sets (L8 and S2 phenological metrics), the RF classification was performed to predict agricultural land cover types in both studied areas.

We examine and compare the RF models accuracy and maps performance using two assessment indicators. First, we present OOB error results for the two classification approaches as a reliable measure of classification accuracy to examine the model's efficacy [43, 80]. Second, we used the accuracy assessment statistics such as OA, kappa statistic, UA, PA, and F1-score to evaluate and compare the quality of the classification.

In general, the lowest OOB error of 6.35% was obtained by the model of classification based on S2 Phenological metrics. These values indicate that the RF model performs effectively and consistently. For the classification based on L8 data, the OOB error increased by 3% to reach 9.63%. Moreover, our results are more accurate than those obtained by Wang et al. [80]. The classification accuracy statistics obtained for crop classes on each classification scheme is shown in Table 4.

The results showed that the classification based on Sentinel-2 phenological data was slightly more accurate with the highest overall accuracy of 93% and a kappa coefficient of 0.91. This compares with an overall classification accuracy and a Kappa coefficient of 90% and 0.88, respectively, for the classification based on the L8 phenological data. This observation confirms the results reported by previous studies of crop and land cover mapping using S2 and L8 data [42, 72, 74, 80] in which classification accuracies obtained from Sentinel-2 data are higher than the results of Landsat-8 data. It is important to realize that even though the number of classes used in our study was relatively large (i.e., 12 classes in total), our results produced a high overall accuracy compared to other studies conducted in the same context but with fewer classes. The work by Bendini et al. [8] reported a similar crop classification accuracies using L8 phenological data for mapping four classes of crops in Brazil. In another study, El Mansouri et al. [23] achieved an overall accuracy of 80% using the data fusion of Sentinel-1A and Sentinel-2 to identify seven crop classes in the Triffa Plain.

When discussing and comparing the accuracies of individual crop types on each classification approaches, we can see that the classification has achieved satisfactory accuracies among the different classes. However, the low accuracies for some classes can be seen critical for crop mapping. In particular, the pomegranate, which always shows the lowest PA, F1-score, and the UA, could be caused by two main reasons. On the one hand, as shown in Table 1, we could find that the pomegranate class was poorly represented in the studied regions during the season of 2016/2017. On the other hand, the main reason for the recorded low F1-score PA and UA was the similar spectral

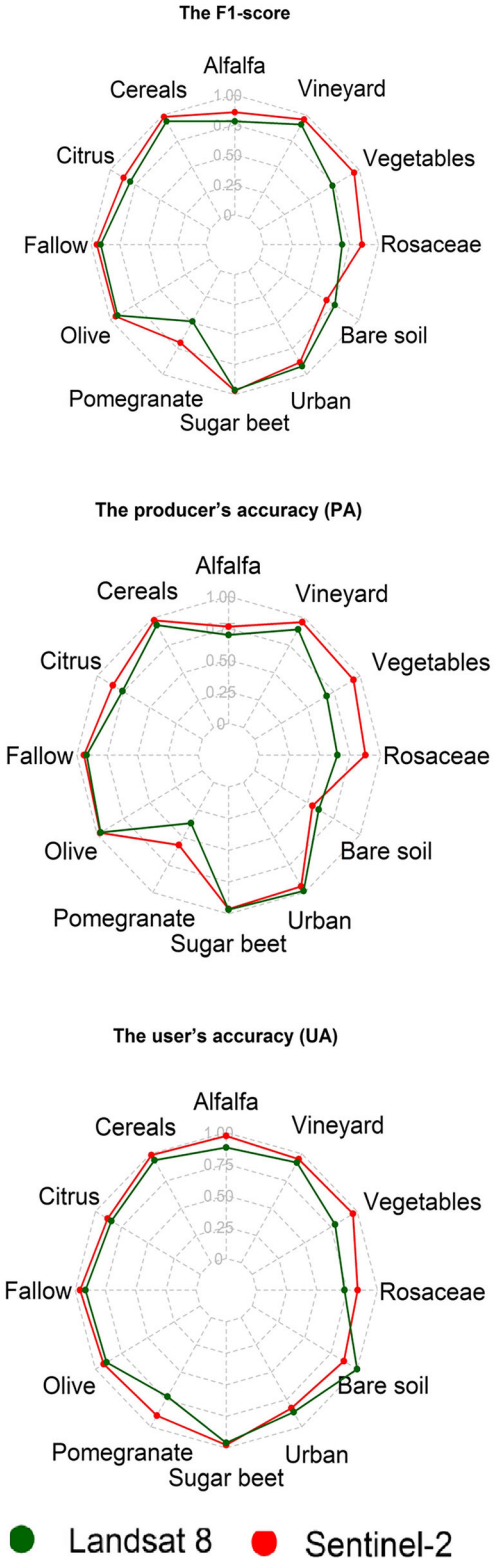

Fig. 8 Spider charts representing the user's accuracies, producer accuracies, and the F1-score for the following classification based on Landsat-8 and Sentinel-2 phenological metrics

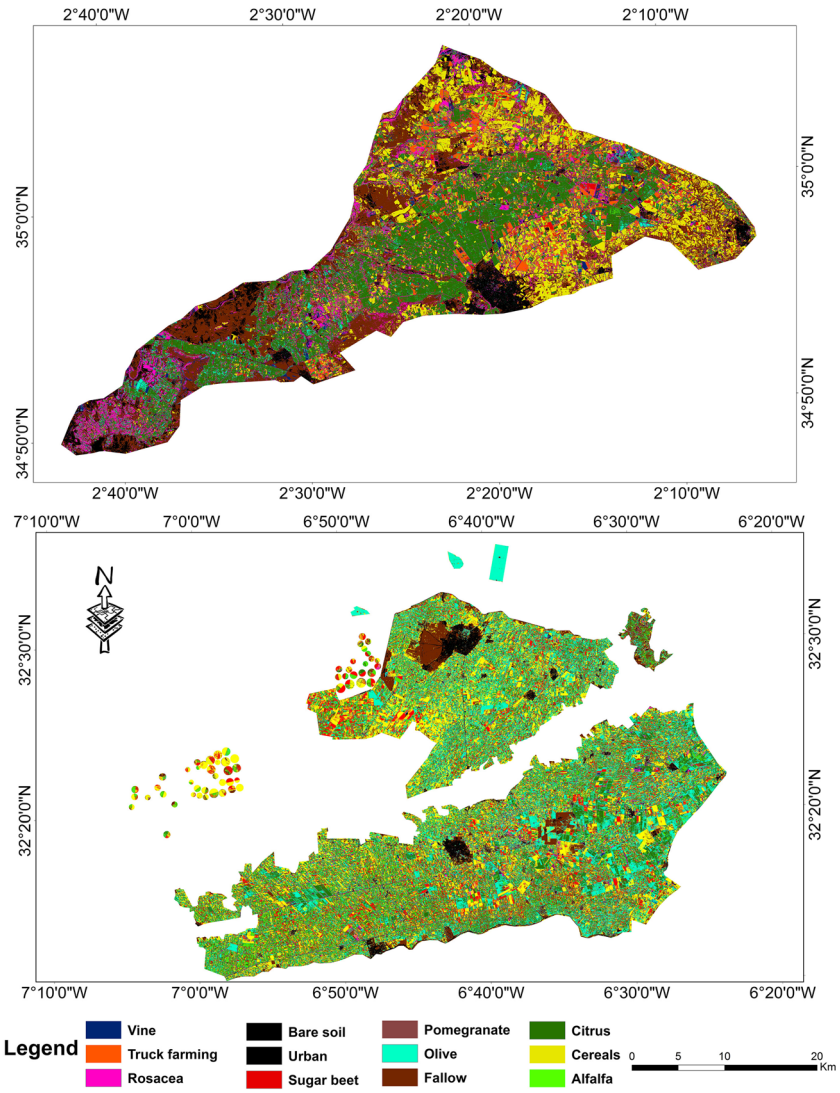

Fig. 9 Final crop type maps over the (a) Triffa and (b) Tadla irrigated perimeters obtained by Random Forest classification based on phenological metrics data derived from Sentinel-2

behavior of some of the crops with the pomegranate classes as shown in Fig. 4. The same limits can be explained by many other studies [50, 52] reporting that the number of training samples significantly affects the classification results.

Figure 8 summarizes the comparison between the two classification approaches based on the PA, UA, and F1-score per crop types. As can be seen from this figure, it is clear the effect of using the phenological metrics derived from S2 data compared to those derived from L8. The classes of rosaceae, vegetables, vineyard, and alfalfa have potentially benefited from the added value of S2 variables, with a significant increase in user's and producer's accuracies in addition to the F1 score. Nevertheless, using the Sentinel-2 phenological data for the crop classes of olives, sugar beets, and fallow did not increase the classification accuracies of these crops.

Figure 9 shows the resultant maps of crop classification. They show the distribution of cropland types and crop classes distinguishable at 10-m spatial resolution.

After assessing the quality of the classification result, this study have demonstrated that the classification approach using the phenological data derived from Sentinel-2 achieves a higher classification accuracy than the Landsat phenological data in most classes.

These results were also confirmed through the visual comparison and interpretation of a subset classified maps based on L8 and S2 data using ground data training (Fig. 10). In general, the fields have been classified correctly for both sensors data; however, the crops mapped using the Sentinel-2 data are spatially more consistent over the study areas than those mapped using L8 images, which offers a more clearer visual appearance and an esthetic depiction of cropland types. This observation confirms the results obtained by Labib and Harris [42] and Wang et al. [80], who reported the advantages of S2 data due to its slightly higher spatial resolution.

The final crop type map over the Triffa and Tadla irrigated perimeters (Fig. 9) is used to estimate and provide crop area

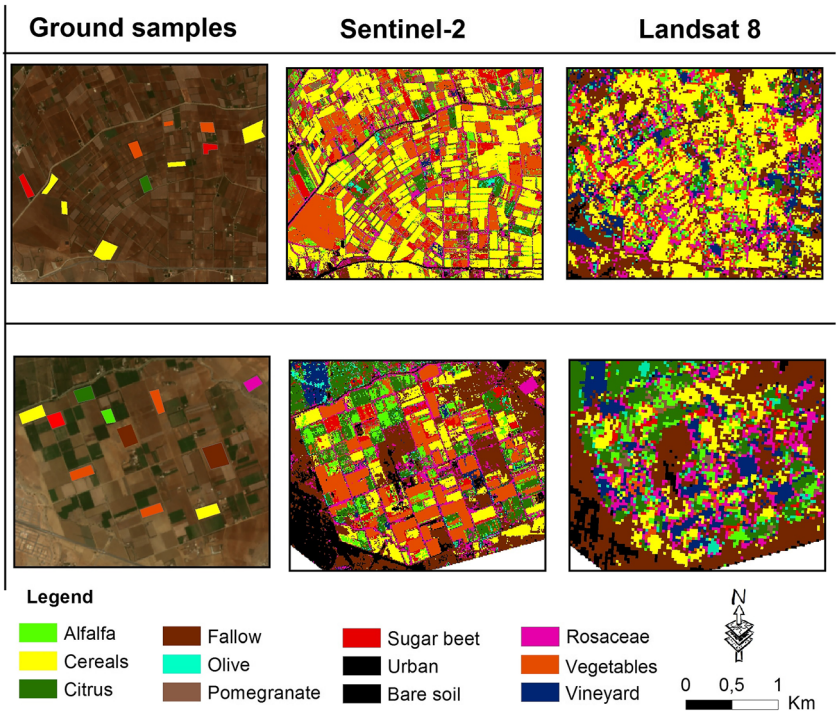

Fig. 10 A visual comparison of the RF classification results based on Landsat 8 and Sentinel-2 phenological metrics of a zoomed area in the Triffa irrigated perimeters site using the overlay of the ground/field data

statistics in thousands of hectares (Kha) for each study area (Fig. 11).

The crop area values presented in Fig. 11 show that the cropping systems dominating in the irrigated perimeter of Tadla were olive, and they covered more than 26% of total cropland area. Citrus and sugar beet were the next dominant systems accounting for 21% and 17% of the cropland area, respectively. On the other side, the Triffa irrigated perimeter is characterized by crop diversification with the following values as shown in Fig. 11: citrus (24%), fallow (23%), cereals (15%), vegetables (9%), and alfalfa (4%). The area statistics derived from classification results were compared to the available official statistics of ORMVAM and ORMVAT (Table 5).

Table 5 shows that the satellite-derived crop areas present a good agreement with the updated official statistics. If we take the example of citrus in Triffa, the obtained final area estimates agree with official statistics for 2017, which indicate a citrus area of 19,800 ha. The same correspondence was observed for the olive and sugar beet in Tadla with a relative error of − 4.48 and − 1.3, respectively. Unfortunately, the other

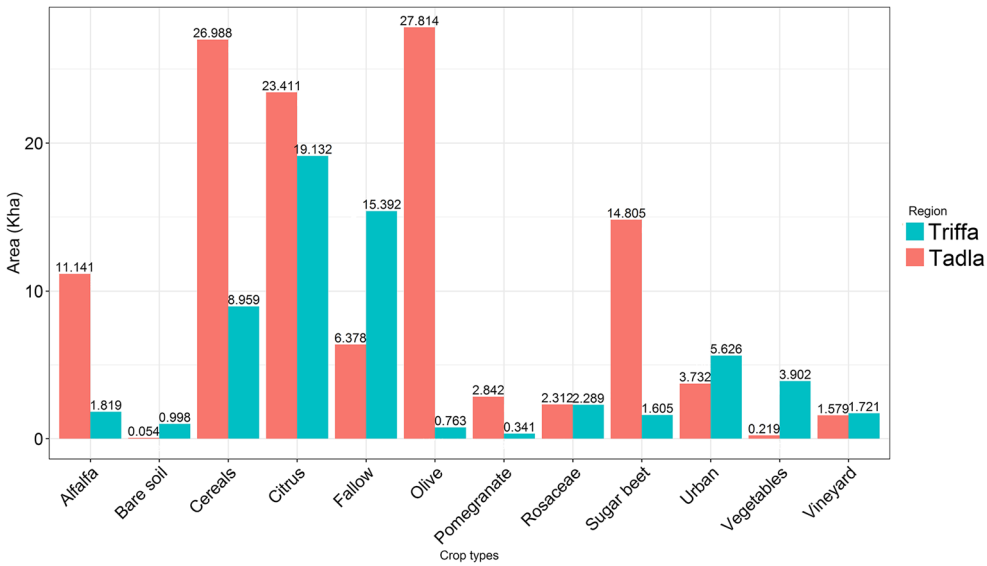

Fig. 11 Area statistics (in Kha) derived from the random forest classification of Tadla and Triffa irrigated perimeters

Table 5 Cross-comparison of official statistics and major crop area estimates derived from Sentinel-2 data over the irrigated perimeters

Classes	Crop area: official statistics	Crop area: Sentinel-2 derived	Relative error (%)
Triffa region			
Citrus	19,800	19,132	− 3.3
Tadla region			
Sugar beet	15,000	14,805	− 1.3
Olive	26,620	27,814	− 4.48

crop area estimates could not be compared due to the lack of official statistics at study areas; in general, these are not updated regularly on an annual basis, which made comparisons difficult and prevented validation to be performed.

The high accuracy obtained for the result maps demonstrates the effectiveness and reliability of the proposed approach based on phenological metrics derived from remote sensing time series. This approach can be accurate, updatable, and cost-effective for mapping and monitoring cropland compared to conventional methods and surveys that are subjective, time-consuming, and laborious.

5 Conclusions and Perspectives

Crop identification and mapping are extremely important for numerous environmental planning and research applications. Remote sensing offers an efficient and reliable means of collecting and creating information. Satellite-derived cropland products and information can provide valuable, real-time advice for sustainable agricultural development strategies and natural resources protection as it increases the possibility of large-scale operational mapping of cropland with high spatio-temporal resolution. The use of satellite imagery from a single source can be limited by the presence of clouds and shadows that introduce missing values in the datasets in addition to the difficult for capturing the seasonality of the vegetation cover. Based on this issue, our study focused on evaluating the potential of phenological metrics derived from the Sentinel-2A (S2) and Landsat 8 (L8) data in classifying and mapping crop type for two study areas in Morocco. We used the TIMESAT tools first to smooth the times series of NDVI by the Savitzky–Golay filter and second to extract phenological metrics from the smoothed NDVI time series. A supervised Random Forest classifier (RF) was used to select and optimize these phenological parameters and perform the classification by employing the selected features based on the Mean Decrease in Accuracy (MDA) approach.

The results show that the classification based on phenological metrics derived from S2 achieved a satisfactory overall classification accuracy and Kappa coefficient of 93% and 0.91, respectively. In comparison, the approach that used L8 phenological metrics had an overall classification accuracy and kappa coefficient decreased by 3%. The producer's accuracy, the user's accuracy, and F1-score improved for most crop types in the classification based on S2 compared to L8 phenological information.

The approach presented can potentially be replicated in other regions in Morocco and the world to identify crops. Our results prove that this data has the ability to produce accurate maps of relevant farming systems, especially with the launch of new satellites such as Sentinel-2B. These images are now provided on a 5-day basis. Also, they should improve the availability of input data (NDVI Series) and facilitate subsequent applications of the approach developed for crop mapping. This is in spite of the data volume to be processed that involves a very long computation time and a limitation in terms of memory limits of the software used.

Finally, this research allowed us to map the major crop classes in the irrigated perimeters of Tadla and Triffa in Morocco. It is important, in perspective, to establish complementary research to improve this approach for mapping crops at national and regional scale.

References

1. Abad M, Abkar A, Mojaradi B (2018) Effect of the temporal gradient of vegetation indices on early-season wheat classification using the random forest classifier. Appl Sci 8:1216. https://doi.org/10.3390/app8081216
2. Alganci U, Sertel E, Ozdogan M, Ormeci C (2013) Parcel-level identification of crop types using different classification algorithms and multi-resolution imagery in southeastern Turkey. Photogramm Eng Remote Sens 79:1053–1065. https://doi.org/10.14358/PERS.79.11.1053
3. Bannari A, Morin D, Bonn F, Huete AR (1995) A review of vegetation indices. Remote Sensing Reviews 13:95–120. https://doi.org/10.1080/02757259509532298
4. Bastiaanssen WGM, Molden D, Makin I (2000) Remote sensing for irrigated agriculture: examples from research and possible applications. Agric Water Manag 46:137–155. https://doi.org/10.1016/S0378-3774(00)00080-9
5. Belgiu M, Csillik O (2018) Sentinel-2 cropland mapping using pixel-based and object-based time-weighted dynamic time warping analysis. Remote Sens Environ 204:509–523. https://doi.org/10.1016/j.rse.2017.10.005
6. Belgiu M, Drăguț L (2016) Random forest in remote sensing: a review of applications and future directions. ISPRS J Photogramm Remote Sens 114:24–31. https://doi.org/10.1016/j.isprsjprs.2016.01.011

7. Benabdelouahab T, Balaghi R, Hadria R et al (2016) Testing Aquacrop to simulate durum wheat yield and schedule irrigation in a semi-arid irrigated perimeter in Morocco: testing Aquacrop to simulate durum wheat yield and schedule irrigation. Irrig Drain 65: 631–643. https://doi.org/10.1002/ird.1977
8. Bendini H, Sanches ID, Körting TS et al (2016) Using Landsat 8 image time series for crop mapping in a region of Cerrado, Brazil. ISPRS - Int Arch Photogramm Remote Sens Spat. Inf Sci XLI-B8: 845–850. https://doi.org/10.5194/isprsarchives-XLI-B8-845-2016
9. Benhadj I, Duchemin B, Maisongrande P et al (2012) Automatic unmixing of MODIS multi-temporal data for inter-annual monitoring of land use at a regional scale (Tensift, Morocco). Int J Remote Sens 33:1325–1348. https://doi.org/10.1080/01431161.2011.564220
10. Bernard S (2009) Forêts Aléatoires: De l'Analyse des Mécanismes de Fonctionnement à la Construction Dynamique. Phd diss, Université de Rouen
11. Biradar C, Thenkabail P, Noojipady P et al (2009) A global map of rainfed cropland areas (GMRCA) at the end of last millennium using remote sensing. Int J Appl Earth Obs Geoinformation 11: 114–129. https://doi.org/10.1016/j.jag.2008.11.002
12. Breiman L (2001) Random forests. Mach Learn 45:5–32. https://doi.org/10.1023/A:1010933404324
13. Brooks CN, Schaub DL, Powell RB et al (2006) Multi-temporal and multi-platform agricultural land cover classification in southeastern Michigan. In: proceedings of ASPRS 2006 annual conference. Reno, Nevada, p 12
14. Chen J, Jönsson P, Tamura M et al (2004) A simple method for reconstructing a high-quality NDVI time-series data set based on the Savitzky–Golay filter. Remote Sens Environ 91:332–344. https://doi.org/10.1016/j.rse.2004.03.014
15. Clark ML (2017) Comparison of simulated hyperspectral HyspIRI and multispectral Landsat 8 and Sentinel-2 imagery for multi-seasonal, regional land-cover mapping. Remote Sens Environ 200: 311–325. https://doi.org/10.1016/j.rse.2017.08.028
16. Cohen J (1960) A coefficient of agreement for nominal scales. Educ Psychol Meas 20:37–46. https://doi.org/10.1177/001316446002000104
17. Congalton RG (1991) A review of assessing the accuracy of classifications of remotely sensed data. Remote Sens Environ 37:35–46. https://doi.org/10.1016/0034-4257(91)90048-B
18. Defries R, Townshend J (1994) NDVI-derived land cover classification at a global scale. Int J Remote Sens - INT J REMOTE SENS 15:3567–3586. https://doi.org/10.1080/01431169408954345
19. Drusch M, Del Bello U, Carlier S et al (2012) Sentinel-2: ESA's optical high-resolution Mission for GMES operational services. Remote Sens Environ 120:25–36. https://doi.org/10.1016/j.rse.2011.11.026
20. Durgun YÖ, Gobin A, Van De Kerchove R, Tychon B (2016) Crop area mapping using 100-m Proba-V time series. Remote Sens 8: 585. https://doi.org/10.3390/rs8070585
21. Eklundh L, Jönsson P (2012) TIMESAT 3.1 software manual. Lund Univ Swed 1–82
22. El Mansouri L (2013) Object-based approach and tree-based ensemble classifications for mapping building changes. In: Proceedings of the fifth international conference on advanced geographic information systems, applications, and services GEOProcessing, Nice, pp 54–59
23. El Mansouri L, Lahssini S, Hadria R et al (2019) Time series multispectral images processing for crops and Forest mapping: two Moroccan cases. In: El-Ayachi M (ed) El Mansouri L. Geospatial Technologies for Effective Land Governance, IGI Global, pp 83–106
24. Friedl MA, Brodley C (1997) Decision tree classification of land cover from remotely sensed data. Remote Sens Environ 61:399–409. https://doi.org/10.1016/S0034-4257(97)00049-7
25. Genuer R, Poggi J-M, Tuleau-Malot C (2010) Variable selection using random forests. Pattern Recogn Lett 31:2225–2236
26. Gómez C, White JC, Wulder MA (2016) Optical remotely sensed time series data for land cover classification: a review. ISPRS J Photogramm Remote Sens 116:55–72. https://doi.org/10.1016/j.isprsjprs.2016.03.008
27. Haerani H, Apan A, Basnet B (2018) Mapping of peanut crops in Queensland, Australia, using time-series PROBA-V 100-m normalized difference vegetation index imagery. J Appl Remote Sens 12:1. https://doi.org/10.1117/1.JRS.12.036005
28. Hagolle O, Dedieu G, Mougenot B et al (2008) Correction of aerosol effects on multi-temporal images acquired with constant viewing angles: application to Formosat-2 images. Remote Sens Environ 112:1689–1701
29. Hagolle O, Huc M, Pascual DV, Dedieu G (2010) A multi-temporal method for cloud detection, applied to FORMOSAT-2, VENμS, LANDSAT and SENTINEL-2 images. Remote Sens Environ 114: 1747–1755
30. Hagolle O, Huc M, Villa Pascual D, Dedieu G (2015) A multi-temporal and multi-spectral method to estimate aerosol optical thickness over land, for the atmospheric correction of FormoSat-2, LandSat, VENμS and Sentinel-2 images. Remote Sens 7:2668–2691
31. Hao P, Wang L, Zhan Y, Niu Z (2016) Using moderate-resolution temporal NDVI profiles for high-resolution crop mapping in years of absent ground reference data: a case study of bole and Manas counties in Xinjiang, China. ISPRS Int J Geo-Inf 5:67. https://doi.org/10.3390/ijgi5050067
32. Heumann BW, Seaquist JW, Eklundh L, Jönsson P (2007) AVHRR derived phenological change in the Sahel and Soudan, Africa, 1982–2005. Remote Sens Environ 108:385–392. https://doi.org/10.1016/j.rse.2006.11.025
33. Immitzer M, Atzberger C, Koukal T (2012) Tree species classification with random Forest using very high spatial resolution 8-band WorldView-2 satellite data. Remote Sens 4:2661–2693. https://doi.org/10.3390/rs4092661
34. Immitzer M, Vuolo F, Atzberger C (2016) First experience with Sentinel-2 data for crop and tree species classifications in Central Europe. Remote Sens 8:166. https://doi.org/10.3390/rs8030166
35. Inglada J, Vincent A, Arias M, Sicre C (2016) Improved early crop type identification by joint use of high temporal resolution SAR and optical image time series. Remote Sens 8:362. https://doi.org/10.3390/rs8050362
36. Irons JR, Dwyer JL, Barsi JA (2012) The next Landsat satellite: the Landsat data continuity Mission. Remote Sens Environ 122:11–21. https://doi.org/10.1016/j.rse.2011.08.026
37. Jeganathan C, Dash J, Atkinson PM (2010) Characterising the spatial pattern of phenology for the tropical vegetation of India using multi-temporal MERIS chlorophyll data. Landsc Ecol 25:1125–1141. https://doi.org/10.1007/s10980-010-9490-1
38. Jonsson P, Eklundh L (2002) Seasonality extraction by function fitting to time-series of satellite sensor data. IEEE Trans Geosci Remote Sens 40:1824–1832. https://doi.org/10.1109/TGRS.2002.802519
39. Jönsson P, Eklundh L (2004) TIMESAT—a program for analyzing time-series of satellite sensor data. Comput Geosci 30:833–845. https://doi.org/10.1016/j.cageo.2004.05.006
40. Kim M, Lee J, Han D et al (2018) Convolutional neural network-based land cover classification using 2-D spectral reflectance curve graphs with multitemporal satellite imagery. IEEE J Sel Top Appl Earth Obs Remote Sens 11:4604–4617. https://doi.org/10.1109/JSTARS.2018.2880783
41. Kussul N, Skakun S, Shelestov A et al (2015) Regional scale crop mapping using multi-temporal satellite imagery. ISPRS - Int Arch Photogramm Remote Sens Spat Inf Sci XL-7(W3):45–52. https://doi.org/10.5194/isprsarchives-XL-7-W3-45-2015

42. Labib SM, Harris A (2018) The potentials of Sentinel-2 and LandSat-8 data in green infrastructure extraction, using object based image analysis (OBIA) method. Eur J Remote Sens 51: 231–240. https://doi.org/10.1080/22797254.2017.1419441
43. Lawrence RL, Wood SD, Sheley RL (2006) Mapping invasive plants using hyperspectral imagery and Breiman cutler classifications (randomForest). Remote Sens Environ 100:356–362. https://doi.org/10.1016/j.rse.2005.10.014
44. Lebrini Y, Boudhar A, Hadria R et al (2019) Identifying agricultural systems using SVM classification approach based on phenological metrics in a semi-arid region of Morocco. Earth Syst Environ 3: 277–288. https://doi.org/10.1007/s41748-019-00106-z
45. Lee E (2014) Analysis of MODIS 250 m NDVI using different time-series data for crop type Separability. PhD diss., University of Kansas
46. Liaw A, Wiener M (2002) Classification and regression by randomForest. R News 2:18–22
47. Lionboui H, Benabdelouahab T, Elame F et al (2018) Estimating the economic impact of climate change on agricultural water management indicators. PERTANIKA J Sci Technol 26:749–762
48. Liu QJ, Takamura T, Takeuchi N, Shao G (2002) Mapping boreal vegetation of a temperate mountain in China by multitemporal Landsat TM imagery. Int J Remote Sens - INT J REMOTE SENS 23:3385–3405. https://doi.org/10.1080/01431160110076171
49. Lobell DB, Asner GP, Ortiz-Monasterio JI, Benning TL (2003) Remote sensing of regional crop production in the Yaqui Valley, Mexico: estimates and uncertainties. Agric Ecosyst Environ 94: 205–220. https://doi.org/10.1016/S0167-8809(02)00021-X
50. Lu D, Weng Q (2007) A survey of image classification methods and techniques for improving classification performance. Int J Remote Sens 28:823–870. https://doi.org/10.1080/01431160600746456
51. Mathur A, Foody GM (2008) Crop classification by support vector machine with intelligently selected training data for an operational application. Int J Remote Sens 29:2227–2240. https://doi.org/10.1080/01431160701395203
52. Maxwell AE, Warner TA, Fang F (2018) Implementation of machine-learning classification in remote sensing: an applied review. Int J Remote Sens 39:2784–2817. https://doi.org/10.1080/01431161.2018.1433343
53. McCloy KR, Lykke AM (2009) Validation of phenological change indices as derived from time series of image data. In: Proceedings of Multitemp 2009. Mistic, Connecticut, pp 307–314
54. Meyer H, Kühnlein M, Appelhans T, Nauss T (2016) Comparison of four machine learning algorithms for their applicability in satellite-based optical rainfall retrievals. Atmospheric Res 169:424–433. https://doi.org/10.1016/j.atmosres.2015.09.021
55. Ouatiki H, Boudhar A, Tramblay Y, et al (2017) Evaluation of TRMM 3B42 V7 rainfall product over the Oum Er Rbia Watershed in Morocco
56. Ozdarici-Ok A, Ok A, Schindler K (2015) Mapping of agricultural crops from single high-resolution multispectral images—data-driven smoothing vs. parcel-based smoothing. Remote Sens 7:5611–5638. https://doi.org/10.3390/rs70505611
57. Pal M, Mather PM (2003) An assessment of the effectiveness of decision tree methods for land cover classification. Remote Sens Environ 86:554–565. https://doi.org/10.1016/S0034-4257(03)00132-9
58. Palchowdhuri Y, Valcarce-Diñeiro R, King P, Sanabria-Soto M (2018) Classification of multi-temporal spectral indices for crop type mapping: a case study in Coalville. UK J Agric Sci:1–13. https://doi.org/10.1017/S0021859617000879
59. Pelletier C, Valero S, Inglada J et al (2016) Assessing the robustness of random forests to map land cover with high resolution satellite image time series over large areas. Remote Sens Environ 187:156–168. https://doi.org/10.1016/j.rse.2016.10.010
60. Price KP, Egbert SL, Nellis MD, et al (1997) Mapping land cover in a high plains agro-ecosystem using a multidate Landsat thematic mapper modeling approach. Trans Kans Acad Sci 1903–100:21–33. doi: https://doi.org/10.2307/3628436
61. Qin C (2011) Assessing phenological changes and drivers in East Africa from 1982 to 2006. PhD diss., Michigan State University
62. Reed BC, Brown JF, VanderZee D et al (1994) Measuring phenological variability from satellite imagery. J Veg Sci 5:703–714. https://doi.org/10.2307/3235884
63. Rengarajan R, Schott J (2018) Evaluation of sensor and environmental factors impacting the use of multiple sensor data for time-series applications. Remote Sens 10:1678. https://doi.org/10.3390/rs10111678
64. Rimal B, Zhang L, Rijal S (2018) Crop cycles and crop land classification in Nepal using MODIS NDVI. Remote Sens Earth Syst Sci 1:14–28. https://doi.org/10.1007/s41976-018-0002-4
65. Rodrigues A, Marcal ARS, Furlan D et al (2013) Land cover map production for Brazilian Amazon using NDVI SPOT VEGETATION time series. Can J Remote Sens 39:277–289. https://doi.org/10.5589/m13-037
66. Rodriguez-Galiano VF, Chica-Olmo M, Abarca-Hernandez F et al (2012a) Random Forest classification of Mediterranean land cover using multi-seasonal imagery and multi-seasonal texture. Remote Sens Environ 121:93–107. https://doi.org/10.1016/j.rse.2011.12.003
67. Rodriguez-Galiano VF, Ghimire B, Rogan J et al (2012b) An assessment of the effectiveness of a random forest classifier for land-cover classification. ISPRS J Photogramm Remote Sens 67:93–104. https://doi.org/10.1016/j.isprsjprs.2011.11.002
68. Rouse JW Jr, Haas RH, Schell JA, Deering DW (1974) Monitoring vegetation systems in the Great Plains with Erts. In: Proceedings of the 3rd earth resource technology satellite (ERTS) symposium, Washington, pp 309–317
69. Roy DP, Li J, Zhang HK et al (2017) Examination of Sentinel-2A multi-spectral instrument (MSI) reflectance anisotropy and the suitability of a general method to normalize MSI reflectance to nadir BRDF adjusted reflectance. Remote Sens Environ 199:25–38. https://doi.org/10.1016/j.rse.2017.06.019
70. Savitzky A, Golay MJE (1964) Smoothing and differentiation of data by simplified least squares procedures. Anal Chem 36:1627–1639. https://doi.org/10.1021/ac60214a047
71. Sonobe R, Yamaya Y, Tani H et al (2018) Crop classification from Sentinel-2-derived vegetation indices using ensemble learning. J Appl Remote Sens 12:1. https://doi.org/10.1117/1.JRS.12.026019
72. Sothe C, Almeida C, Liesenberg V, Schimalski M (2017) Evaluating Sentinel-2 and Landsat-8 data to map successional forest stages in a subtropical Forest in southern Brazil. Remote Sens 9: 838. https://doi.org/10.3390/rs9080838
73. Steenkamp K, Wessels KJ, Archibald S, Von Maltitz GP (2009) Satellite derived phenology of southern Africa for 1985–2000 and functional classification of vegetation based on phenometrics. In: proceedings of the 33rd international symposium of remote sensing of the environment (ISRSE), Stresa, p 4
74. Topaloğlu RH, Sertel E, Musaoğlu N (2016) Assessment of classification accuracies of Sentinel-2 and Landsat-8 data for land cover/use mapping. ISPRS - Int Arch Photogramm Remote Sens Spat Inf Sci XLI-B8:1055–1059. doi: https://doi.org/10.5194/isprsarchives-XLI-B8-1055-2016
75. Tucker CJ (1979) Red and photographic infrared linear combinations for monitoring vegetation. Remote Sens Environ 8:127–150. https://doi.org/10.1016/0034-4257(79)90013-0
76. Vermote E, Justice C, Claverie M, Franch B (2016) Preliminary analysis of the performance of the Landsat 8/OLI land surface reflectance product. Remote Sens Environ 185:46–56

77. Vieira CAO, Mather PM, Aplin P (2002) Multitemporal classification of agricultural crops using the spectral-temporal response surface. In: Bruzzone L, Smits P (eds) Analysis of Multi-Temporal RemoteSensing Images, pp 290–297
78. Vintrou E, Desbrosse A, Bégué A et al (2012) Crop area mapping in West Africa using landscape stratification of MODIS time series and comparison with existing global land products. Int J Appl Earth Obs Geoinformation 14:83–93. https://doi.org/10.1016/j.jag.2011.06.010
79. Vuolo F, Neuwirth M, Immitzer M et al (2018) How much does multi-temporal Sentinel-2 data improve crop type classification? Int J Appl Earth Obs Geoinformation 72:122–130. https://doi.org/10.1016/j.jag.2018.06.007
80. Wang D, Wan B, Qiu P et al (2018) Evaluating the performance of Sentinel-2, Landsat 8 and Pléiades-1 in mapping mangrove extent and species. Remote Sens 10:1468. https://doi.org/10.3390/rs10091468
81. Wardlow BD, Egbert SL (2005) State-level crop mapping in the US Central Great Plains agroecosystem using MODIS 250-meter NDVI data. In: Proceedings of Pecora 16 Symposium, Sioux Falls, South Dakota, pp 23–27
82. Wardlow B, Egbert S, Kastens J (2007) Analysis of time-series MODIS 250 m vegetation index data for crop classification in the U.S. Central Great Plains. Remote Sens Environ 108:290–310. https://doi.org/10.1016/j.rse.2006.11.021
83. Wessels K, Steenkamp K, von Maltitz G, Archibald S (2011) Remotely sensed vegetation phenology for describing and predicting the biomes of South Africa: remotely sensed vegetation phenology of South Africa's biomes. Appl Veg Sci 14:49–66. https://doi.org/10.1111/j.1654-109X.2010.01100.x
84. Zheng B, Myint SW, Thenkabail PS, Aggarwal RM (2015) A support vector machine to identify irrigated crop types using time-series Landsat NDVI data. Int J Appl Earth Obs Geoinformation 34:103–112. https://doi.org/10.1016/j.jag.2014.07.002